SSC25-P1-39

Development of a Polarization-Based Optical Communications Ground Station for the PULSE-A CubeSat

Juan Ignacio Prieto Asbun, Leah Vashevko, Mason McCormack, Rodrigo Spinola e Castro, Ashley Ashiku, Joshua Johnson, Elizabeth Rosario, Kevin Zamudio, Sasha Malysheva, Nusret Efe Ucer, Qihong Wu, Sofia Mansilla, Seth Knights, Logan Hanssler, Mohammad Hassan, Sofia Cavallione, Nguyen Do, Tian Zhong
The University of Chicago
Eckhardt, 5640 S Ellis Ave, Chicago, IL 60637; 872-335-6826
jiprieto@uchicago.edu

ABSTRACT

The Polarization-modUlated Laser Satellite Experiment (PULSE-A) is the University of Chicago's student-led mission to demonstrate an optical downlink at a data rate of 1 to 10 Mbps using circular polarization shift keying (CPolSK). PULSE-A comprises a 3U CubeSat bus carrying a <1.5U optical transmission terminal and a dual optical-RF ground station. The ground station (GS) system consists of the optical ground station (OGS) and the RF ground station (RFGS). The RFGS is responsible for standard communications and control tasks, while the experimental OGS receives the optical transmission from the satellite's payload.

To perform satellite-to-ground optical communications, the OGS needs to track, receive, and decode the transmitted signal while providing its own beacon, which allows the satellite to track the OGS. These requirements are accomplished by four assemblies within the OGS: tracking, polarization state preparation, signal decoding, and beacon. The tracking assembly collects, condenses, and collimates incoming laser light from the satellite using an 11" Schmidt-Cassegrain telescope and an optical assembly, which performs fine tracking of the satellite. The polarization state preparation assembly separates light by its left- or right-handed circularly polarized states. The received circularly polarized transmission laser from the payload passesthrough a quarter-wave plate, converting it into linearly polarized light. This light is then split by a polarizing beam splitter into two separate paths, corresponding to data sent with left- or right-handed circular polarization. Next, the signal-decoding assembly converts the separated polarized light into two voltage channels. These two channels correspond to 1 or 0 bits, which are then digitized by an FPGA. The GS beacon assembly includes the ground beacon laser that enables the satellite to track the ground station.

Since optical communications are directional, the OGS must track the satellite with a pointing accuracy of 1.4 mrad. This requires the GS to conduct a high-precision pointing, acquisition, and tracking (PAT) sequence. First, the RFGS receives telemetry and orbital data, which is passed to the OGS to estimate the satellite's orbital path. The OGS then coarsely points the telescope towards the satellite's predicted position. Then, the satellite illuminates the telescope with a beacon and a transmission laser. The payload beacon laser enables a feedback loop which maintains pointing accuracy by moving the telescope and a fast-steering mirror within the OGS in response to deviations in the laser's position from the center of a tracking camera. This enables the OGS to perform fine corrections to its orbital predictions. As a consequence, the OGS tracks the transmission laser, enabling it to decode the CPolSK transmission.

We present an overview of the design of the GS, focusing on implementing a polarization-based optical communications receiver. This work explores the design of polarization-based optics for space-to-ground optical communications with emphasis on the challenges associated with the directionality of optical communications. We will also cover our independent studies on circular polarization, and how the results affect our design choices.

Mission Overview

Access to high-bandwidth space-to-ground communications is a significant challenge in small form-factor satellite missions. Space-to-ground communications are typically performed with radio frequency (RF) modules, which are capable of high-bandwidth transmission but at the cost of high size, weight, power use, and price. This creates a need for more accessible high-bandwidth communication technology, which can be made possible with laser based optical communications (lasercom). As an added benefit, the directional nature of laser communications makes intercepting transmissions significantly harder, adding an additional layer of security compared to traditional RF.

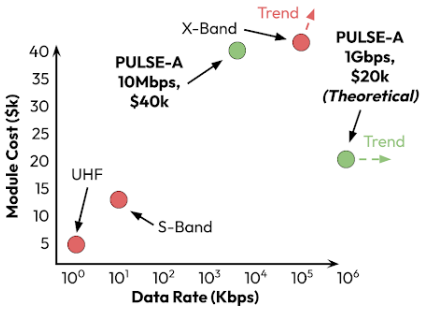

Figure 1: RF and optical communications terminal cost vs data rate

The Polarization modUlated Laser Satellite Experiment (PULSE-A) is the University of Chicago's undergraduate student-led mission designed to demonstrate an optical space-to-ground downlink at a data rate of 1 to 10 Mbps using circular polarization shift keying (CPolSK). In CPolSk, binary data is encoded through the emission of left-handed circularly polarized light for a 1 bit and right-handed circularly polarized light for a 0 bit.

Often, lasercom missions make use of intuitive amplitude modulation schemes, which encode data by switching a laser on and off, or by varying its amplitude. The simplicity of these systems makes them small, light weight, low in power, and robust. Nevertheless, amplitude modulation over long distances in free space optical (FSO) communications is highly susceptible to atmospheric noise and pointing errors; for example, when no signal is detected, it is impossible to distinguish between a 0 bit and an error (Hemmati).

In contrast, polarization shift keying is more complex, but offers greater resistance to interference. For example, since the laser is always on, the receiver is able to differentiate between 0 bits, noise, and missed signals, resulting in a more robust error correction system.

Using linear polarization shift keying (horizontally or vertically polarized light) is inherently challenging as it depends on the relative rotational positions of the optical terminals, which can vary. Circular polarization, however, eliminates such challenges as it is invariant under rotations; furthermore, models suggest anisotropic atmospheric turbulence has little effect on circular polarization states (Su).

This paper will focus on the design and validation of PULSE-A's ground station (GS). The GS serves a dual purpose and is thus split into two subsystems, accordingly: the Radio Frequency Ground Station (RFGS) and the Optical Ground Station (OGS). The RFGS will be responsible for transmitting commands to the satellite and receiving critical telemetry from the satellite health beacon to facilitate accurate tracking for the OGS, sending software updates, enabling the laser communications sequence, and identifying potential issues in the satellite. The OGS will be the receiving end of PULSE-A's experimental polarization modulated optical communications. In order to perform satellite-to-ground optical communications, the OGS must track, receive, and decode the transmitted signal while providing its own beacon, which in turn allows the satellite to track the OGS. Both the use of CPolSK as a modulation scheme and the directionality of optical communications provide major challenges in the design of the OGS, resulting in a unique, high precision dual-channel optical communications receiver.

Both the OGS and the RFGS are designed with more than PULSE-A in mind. The PULSE-A mission as a whole acts as a technological predecessor to the PULSE-Q mission, which intends to demonstrate satellite-to-ground quantum key distribution (QKD).

System Design and Engineering

RFGS Design

The RF system is designed to maintain a strong link to the satellite, and to allow for frequent health beacon and GPS data transmission in order to support the experimental laser communications operations.

All RF communications will be conducted in the amateur UHF band at a frequency between 435 and 438 MHz using a half-duplex system. We will use a Cross-Yagi antenna for its high gain and ease of use, which will be connected to a roof mount with a

Yaesu G-5500 rotator controlled by the CSN Technologies Self-contained Antenna Tracker. The uplink and downlink will be supported by the ICOM-9700 transceiver, with a SSB SP70 masthead preamplifier connected to a DCW 2004 B power coupler to boost weak signals from the satellite. The Cross-Yagi antenna will transmit right-handed circularly polarized RF signals at 30 Watts and receive linearly polarized RF signals from the satellite. While this polarization mismatch will decrease the strength of the received signal by approximately 3 dB, the combination of circular transmission and linear reception will ensure reliable signal reception from the satellite regardless of its orientation.

The RFGS will be capable of receiving telemetry and sending commands and files using the AX.25 standard amateur radio protocol, which will wrap CubeSat Space Protocol (CSP) packets containing command and telemetry data. It will receive and transmit at 9600 baud using GFSK modulation. Packets will be decoded using a Kantronics 9612 XE hardware terminal node controller (TNC) and a ground station computer. The KISS protocol will be used to transmit packets more efficiently between the TNC and computer.

We plan to operate with an FCC experimental license in the amateur UHF band. In accordance with FCC guidelines and recommendations, all uplink commands will be encrypted to maintain operational integrity using a rotating cipher key, while our downlink health beacon will be unencrypted so that it can be received worldwide by amateur radio operators.

We intend to deploy the RFGS on the roof of the Knapp Center for Biomedical Discovery at the University of Chicago. This location will give the antenna an unobstructed line-of-sight for the satellite's orbit. This location will enable the RFGS to connect with the satellite at an elevation of less than 5 degrees, allowing the RFGS to initiate the pointing, acquisition, and tracking (PAT) sequence before the satellite is high enough to begin optical transmission.

Our RF link-budget analysis indicates margins of 21.7 dB on the uplink and 20.3 dB on the downlink, ensuring a strong, reliable signal path for all mission phases.

OGS Design

To perform satellite-to-ground optical communications, the OGS needs to track, receive, and decode the transmitted signal. Simultaneously, it must provide its own beacon at a wavelength of 1064 nm in order for the satellite to be able to track the OGS. The satellite's Payload transmits two beacons: a 1550 nm transmission laser and a 638 nm beacon laser. This three-laser system is at the core of PULSE-A's design.

In order for the OGS to function as a receiving terminal for polarization-based optical communications, it must satisfy the following requirements on pointing, tracking, and decoding laser transmissions:

- The OGS shall transmit the ground station laser beacon to the satellite.
- The OGS shall point to the satellite.
- The OGS shall track the Payload beacon laser.
- The OGS shall detect the downlink transmission laser's wave packets as bits based on separated polarization states.
- The OGS shall decode the downlink transmission laser into digital data.

These system requirements are accomplished by four assemblies within the OGS: Tracking, Polarization State Preparation, Signal Decoding, and Beacon.

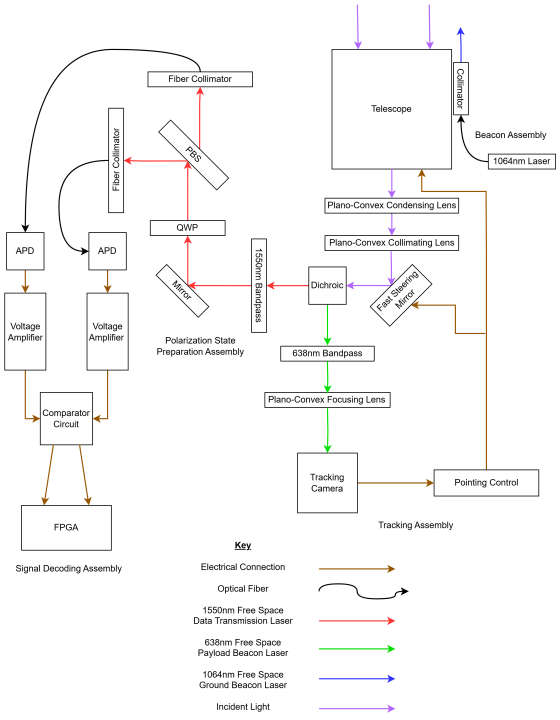

Figure 2: Optical Ground Station Diagram

The following section will describe the design of each of these assemblies, our current progress in the detailed design of each, and our plans for their validation according to the systems requirements outlined above.

Tracking Assembly

The OGS Tracking Assembly collects, condenses, collimates and tracks incoming laser light from the satellite. The assembly uses an 11" Schmidt-Cassegrain telescope—the Celestron CPC 1100—to point at the satellite and collect light. Light is focused onto a custom collimating setup composed of two plano-convex lenses in order to minimize the light's beam waist. The beam then passes through a fast steering mirror (FSM), which is used to center the transmission beam on the receiving photodetectors in the Signal Decoding Assembly. A tracking camera tracks the Payload beacon laser by using a feedback loop; the loop determines the beacon laser's position from the center of the image and uses this information to adjust both the telescope and FSM pointing.

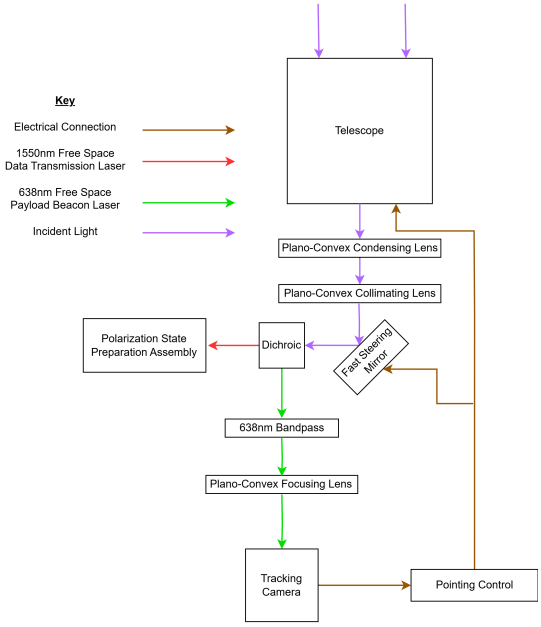

Figure 3: Tracking Assembly Diagram

PAT

In order to create a successful space-to-ground optical link, the satellite and ground station must perform a pointing, acquisition and tracking (PAT) sequence. Simply put, the PAT sequence requires the satellite and ground station to track each other's beacon lasers. On the ground, the OGS will point its telescope at the satellite's predicted location based on orbital predictions and GPS data. Then, it will wait to detect the Payload beacon laser. Once the OGS's tracking camera detects the Payload beacon laser, a feedback loop will be initiated which shifts the FSM by a given angle based on the distance of the beacon to the center of the camera's field of view (FOV). Then, when the pointing error accumulates (i.e. the beacon is off center and the FSM is already tilted near its maximum throw), the feedback loop commands a pointing adjustment for the telescope. This process centers the transmission laser onto the photodetectors used to receive data. Hence, the PAT sequence requires the use of two pointing schemes: coarse pointing, which slews the telescope to detect the Payload beacon, and fine pointing, which moves the FSM to center the light from the transmission laser onto the photodetectors.

Telescope Control

We plan to utilize TLE and GPS data, sent down to the RFGS on previous satellite passes, to predict the satellite's orbit in Earth-centered Cartesian coordinates. The OGS's location will then be used to generate the satellite's altitude and azimuth (azm-alt) coordinates as functions of time.

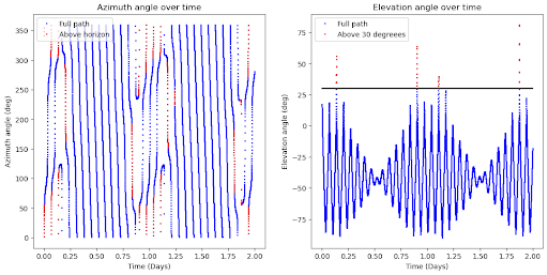

Figure 4: Simulation of azm-alt angles over time for the ISS and OGS located in Chicago, Illinois with points at even time intervals over the course of two days.

To fulfill the course tracking requirement, we will use these azm-alt coordinate predictions to control the telescope. Following alignment, the telescope is controlled via serial communication, using two commands: querying the telescope's current azm-alt coordinates and setting the slew rates in both angular coordinates. Sending both commands takes a non-negligible amount of time in the 50-100 millisecond range, with the nature of serial communication allowing for only one of the commands to be executed at a time. As a consequence, slew rates cannot be sent continuously and must thus be sent at a set time interval. By linearly approximating the azm-alt coordinates for the pass, we obtain their time derivatives, which we can use to send slew rates to the telescope while taking into account its angular acceleration. This leads to root mean squared (RMS) errors of about 0.1 degrees in both coordinates—mostly a consequence of the discontinuity of the slew rates.

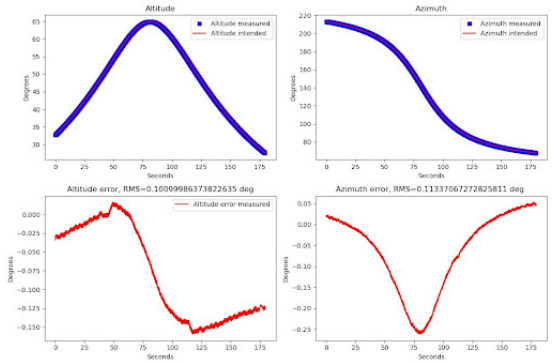

Figure 5: Top plots: Calculated azm-alt for an ISS pass (red) and measured azm-alt (blue) during an attempt to slew the OGS according to the predicted ISS position. Bottom plots: Angular error in both coordinates, taken as the difference between the intended and measured angular positions.

At this point, we can already implement a simple error correction scheme. By computing the angular difference between where the OGS ought to be pointing and where we measure it to be, we can adjust the next slew rate sent to the OGS to correct for this difference. Specifically, we apply a corrective slew rate of $\alpha\frac{\vec{\theta_e}-\vec{\theta_m}}{\Delta t}$, where θ_e is the expected angular position of the satellite, θ_m is the measured angular position of the OGS, Δt is the time interval between slew rate updates, and α is a constant we fine-tune to minimize RMS in each coordinate.

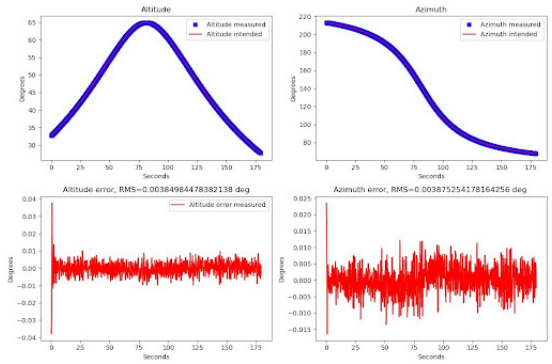

Figure 6: Top plots: Calculated azm-alt for an ISS pass (red) and measured azm-alt (blue) during an attempt to slew the OGS according to the predicted ISS position with correction scheme active and $\alpha = 2$. Bottom plots: Angular error in both coordinates, taken as the difference between the intended and measured angular positions, again with correction scheme active and $\alpha = 2$.

Initially, the telescope will only be moved by the coarse pointing algorithm, which should be sufficient to detect the Payload beacon. Once that has been achieved, we will obtain an offset angle from the position of the Payload beacon's beam on the tracking camera and slew both the telescope and the FSM accordingly to minimize said offset angle. This fine tracking allows us to couple light from the tracking assembly onto our detectors. Our algorithm for this control has not been formulated yet, but we will be using Riesing's algorithm as a base for its development.

Payload Beacon Link Budget

When using a camera—or any sort of detector—there are several sources of noise that need to be accounted for. A link budget allows us to analyze each noise source independently and combine them to determine our expected total noise. In doing so, we will be able to determine the signal strength required to obtain our desired signal-to-noise ratio (SNR).

A priori, we would need to consider the camera's internal and external noise factors. However, in our case, the external noise is negligible since we will be tracking the satellite against the night sky, and the intensity of other sources of light will pale in comparison to the beacon laser. Hence, we have limited our focus to the internal detector noise.

The difficulty in creating the link budget has been that the cameras we are considering are used primarily for astrophotography; they do not have the same listed noise figures as other detectors, such as photodiodes. We've then produced an apparent magnitude calculation for the Payload beacon, showing its apparent magnitude should be around 7. This measurement, however, is insufficient because the apparent magnitude can only provide information about the light source, not the camera. Instead, we have chosen to model the noise directly based on the internal circuit elements.

We are interested in cameras using CMOS image sensors, for which the internal sources of noise are well documented (Tian). We will primarily be focusing on thermal, shot, and 1/f noise. Thermal noise arises from the random thermally induced motion of electrons in the material. Shot noise is generated by the random fluctuations of charge carriers. 1/f noise comes from many of the internal circuit elements, which are all approximately inversely proportional to the frequency of the signal being measured. We can model these sources using probability distributions and then implement them into the link budget. They can then be coupled with the signal sent from the Payload to produce an expected SNR. This expected value will then be used to select our tracking camera, since we need the SNR to fall within a link margin of 3-6 dB.

Tracking Camera

The tracking camera is first used to identify the instance the satellite moves into the telescope's field

of view (FOV) and its Payload beacon becomes detectable. Up until this point, the telescope will have been open-loop tracking the expected orbital path of the satellite, using only the TLEs and GPS data. Acquisition of the satellite will mark the transition from open to closed-loop tracking and coarse to fine-pointing. We expect identification of the Payload beacon to be fairly straightforward; there will be no objects of comparable brightness as a result of the 638nm bandpass filter and extremely short exposure times (< 1 second). Another layer of redundancy to ensure accurate identification of the satellite is that stars can be considered stationary in comparison to our satellite-OGS system. Therefore, any bright object visible over multiple frames must be the satellite. While we do anticipate the Moon or Jupiter to appear brighter than our satellite, passes over the Moon will not be considered optically viable. We will also account for potential acquisition errors from Jupiter in our acquisition code. For fine pointing, the tracking camera's goal is to keep the Payload beacon centered in its FOV. Our tracking code will identify the pixel distance between the center pixel and Payload beacon. This distance will be conveyed to the telescope and FSM for reactionary adjustments and will be completed for each successive image taken during closed-loop tracking. Should there be no bright object viewed across several frames–in other words,the satellite has left the FOV of the telescope– the OGS will revert back to open-loop tracking. To track the satellite, we are considering the usage of the ZWO 1600MM Pro Monochrome camera. The 1600MM Pro has a lowest exposure time of 32 microseconds, which is suitable to take low-exposure frames of our satellite. Since the camera is used purely for tracking a single 638nm beacon laser, color data is not needed and a monochrome camera is most efficient. We chose ZWO brand cameras due to the simplicity of their camera-user interface (ZWO cameras' Software Development Kits (SDK) are published online and there is ample documentation and Python wrappers available). As we write our own Python software, ease of connection and the existence of pre-written Python wrappers for camera commands is a large priority. We have been practicing with a ZWO 1600MM Pro and have achieved connection, camera setting alteration, and image capturing and calibration. Our telescope model contains built-in, fully automated alignment procedures, the most useful being Sky Align. This is our current method of alignment, but if we run into issues of accuracy, we will incorporate our tracking camera in order to perform a plate solve prior to our observation of an optical pass. Furthermore, we expect to automatically calibrate all frames to reduce the signal-to-noise ratio in a calibration method similar to astrophotography with bias, dark, and flat frames taken prior to observing. This simple calibration, along with the identification of the Payload beacon and its distance from the FOV center, is expected to take a negligible amount of time in providing tracking feedback to the FSM and telescope.

ISS Tracking

To verify that the OGS's tracking assembly functions optimally and is capable of tracking the satellite to our desired accuracy, we will reproduce Riesing's tracking of the ISS. This consists of predicting an ISS pass with NORAD TLEs, coarse tracking to a degree of precision where the ISS enters the tracking camera's FOV, and then using fine tracking to keep the ISS centered in the tracking camera FOV. In this experiment, the angular error is measured from the location of the ISS on the tracking camera and our optical setup's plate scale.

Polarization State Preparation Assembly

The polarization state preparation assembly separates light by its left- or right-handed circularly polarized states. It first splits the incoming light from the telescope assembly into the Payload beacon and transmission lasers based on their wavelengths. This split is accomplished by using a dichroic, which diverts the beacon laser into the tracking assembly while passing the transmission laser into the polarization state preparation assembly. The received circularly-polarized transmission laser is passed through a quarter-wave plate, converting it into linearly polarized light. This light is then split by a polarizing beam splitter (PBS) into two separate paths, corresponding to data sent with left- or right-handed circular polarization. These two beams are then collimated into fibers coupled to high-bandwidth avalanche photodiodes (APDs) in the signal decoding assembly.

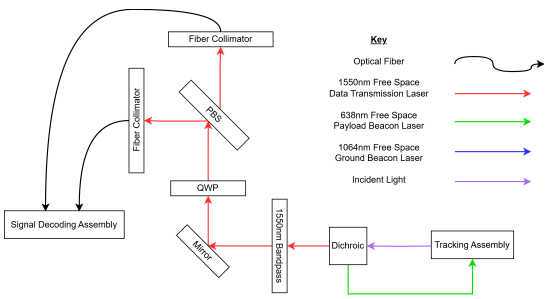

Figure 7: Polarization State Preparation Assembly Diagram

Zemax Simulation and Results

The OGS Zemax simulation uses a ray tracing analysis to validate the optical system and component selection. Zemax is currently used to analyze the FSM's sensitivity to incidence angle in order to determine the acceptable range of beam deviation that will still allow light to couple onto the detectors.

In this simulation, the incoming light source is tilted from the ideal perpendicular angle to imitate a potential deviation. To produce the most accurate results, the maximum angle shift was constrained to prevent significant errors in system performance, such as incorrect polarization or wavelength reaching the detectors due to misalignment. For each angle within this range, irradiance data at the tracking camera and fiber collimators were used to determine the beam centroid's displacement from the center of the detector. The centroid and the incidence angle have a linear correlation and a tolerancing margin of ±0.8°.

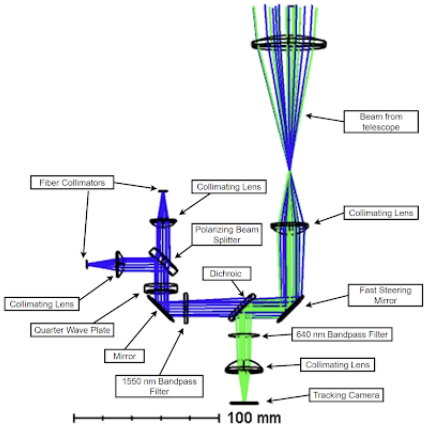

Figure 8: Labeled Zemax simulation of the OGS system

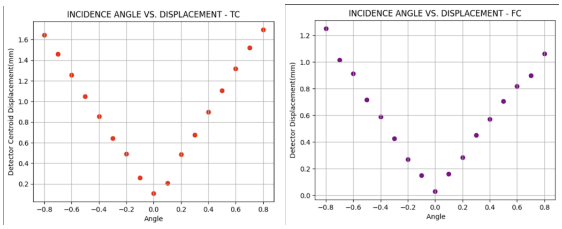

Figure 9: Relationship between FSM incidence angle and detector displacement for the fiber collimators (right) and tracking camera (left).

The limits of the FSM's physical shift were also tested to ensure flexibility in the mirror's movement to accommodate any positional deviations of the beam. To simulate these effects, the FSM's tilt was slightly adjusted until the beam was no longer centered on the following components and began producing damaging back reflections. Similar to the incidence angle test, irradiance centroid data for the tracking camera and fiber collimators were analyzed. The centroid position and FSM tilt show a linear relationship with a functional range of ±1.2°. This indicates that the FSM can compensate for slight hardware misalignments or beam shifts while maintaining proper system performance.

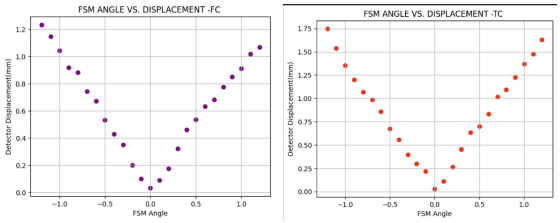

Figure 10: Relationship between FSM tilt and detector displacement for the fiber collimators (left) and tracking camera (right).

The FSM chosen for our optical path is 1 inch in diameter because it is compact enough to fit within the constraints of the setup, but possessing an aperture large enough to allow for tolerancing. If we were to employ a 15 mm FSM to save space, we would observe an increased amount of stray light and back reflections as the FSM would be too small to reflect the entire beam's diameter. A 31 mm FSM would cause more constraint within the system and would allow for a larger range of angles due to its increased size; however, the centroid deviation for the tracking camera is greater within the same ±1.2° and ±0.8° angle ranges. This signifies that the 31 mm FSM has a larger tolerancing margin for both incidence and FSM angle shifts, but there is more power loss at the detectors due to the light being significantly off-center. These comparisons show that the 25.4 mm FSM is ideal for the OGS setup because it optimizes power at the fiber collimators and tracking camera while still maintaining a reasonable range of error.

Our ray tracing analysis conducted with various FSM parameters confirms that the numerical apertures of the fiber collimators are not a limitation for this system. The numerical aperture defines the range of incident angles at which light can be coupled efficiently into the fiber, making it an important factor for beam alignment. The precise collimation provided by the focal lenses ensures that, under proper beam propagation, the light will not enter at an angle approaching the aperture limit. This is significant because it indicates that the system can run with low sensitivity and minimal power loss at the collimators. As a result, the OGS design tolerates a significant margin of error for any skew in the optical setup.

OGS Mechanical Design

The polarization state preparation assembly will be mounted onto the telescope using an optical breadboard with a matte black anodized finish to reduce unwanted reflections. The breadboard will attach to the telescope using custom brackets that attach to the telescope's pre-existing mounting holes. A section of the breadboard will be waterjetted to remove unnecessary weight and ensure that the FSM can receive the incident source from the telescope. The FSM will be mounted at a 45° angle to take the signal into the plane of the optical breadboard. Most optic elements possess large diameters (1 inch) to accommodate the large beam waist of the incoming signal from the second plano-convex lens within the telescope.

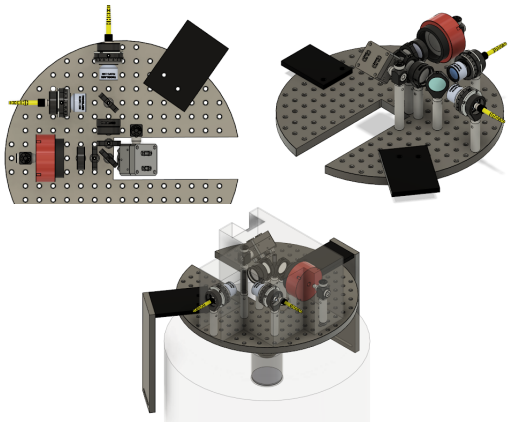

Figure 11: Overhead layout view, isometric view of optics bench, and isometric view of optics bench integrated into the layout.

The polarizing beam splitter (PBS) will differentiate the transmitted signal into two channels based on polarization state, each channel representing a 0 or 1 bit. These signals will be received simultaneously within the two fiber collimators, which couple the light into a single-mode fiber optic cable and transmit the light to its respective fiber-coupled APD. To reduce the strain on fibers when the telescope rotates, we are considering extremely long optical fibers. The APDs and signal decoding assembly will be mounted separately, adjacent to the telescope.

The enclosure serves to block all unnecessary light and environmental hazards, such as wind and dust particles, which could introduce noise or damage optical components, thereby obstructing the process of preparing the polarization state. To minimize costs, the enclosure will be custom 3D-printed. The encasement will feature rubber grommets and seals for fiber optic connections to the collimators and APDs, and likewise for connection to the FSM to ensure proper functionality. The design will be attachable to the breadboard on the optics bench.

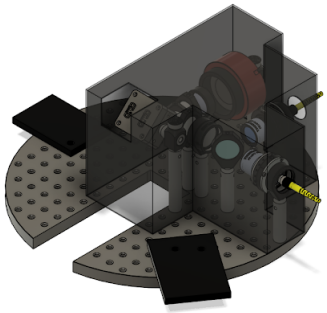

Figure 12: Isometric view of the optical bench with opacity level 60%

A Keplerian beam expander will be mounted within the telescope using plano-convex lenses to ensure proper collimation of incoming light. The objective lens will be securely attached to the bottom of the bore, while the eyepiece lens will be fixed to the telescope's visual back. The beam expander will be positioned directly in the telescope's center.

Figure 13: Side view of the optical layout mounted on the telescope, displaying collimating lenses.

Signal Decoding Assembly

Once the transmission beam is split by left- and right-handed polarization state, the two beams will travel down optical fibers to a pair of avalanche photodiodes (APDs). Due to the low laser power received by the ground station, the output power of the APDs will be on the order of nanovolts and must thus be amplified by a pair of voltage amplifiers.

To mitigate the effects of noise, the resulting signals will be passed through a comparator circuit consisting of two pairs of comparators. The signals corresponding to the left- and right- handed states will each be compared against a threshold voltage,

pulling the channel's signal to ground if the voltage is below the threshold. Simultaneously, the two channels' voltages will be compared to one another. An AND logic gate will be used to guarantee that the incoming signal is both above the threshold and larger than the other channel's signal (within some resolution R).

As a result, the two channels will either both be low when no light is incident to the APDs, or with one channel high and the other low. The target transmission rate of the PULSE-A system is 1-10Mbps, so the OGS must be able to receive, record, and process these signals with at least that speed. This is too fast for traditional microcontrollers, so we will use a field-programmable gate array system (FPGA) which operates at a higher clock speed. FPGAs allow for custom hardware implementations which can operate at nearly arbitrary clock speeds.

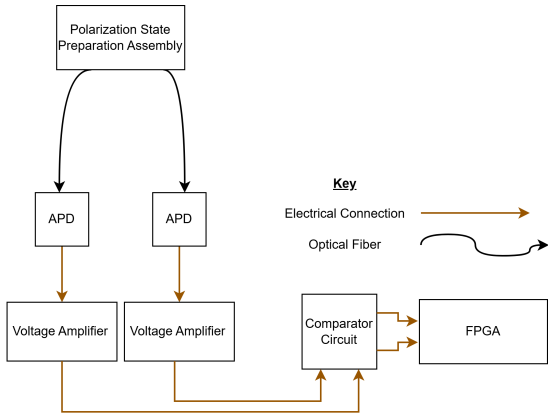

Figure 14: Signal Decoding Assembly Diagram

SNR and Link Budgeting

In order to validate the OGS's capacity to detect and decode a transmitted signal, we need to model its signal-to-noise ratio (SNR). We determine the SNR at the comparator circuit by the following equation: $SNR = \frac{V_{out}}{N_{amplifier}+N_{APD}+N_{external}}$. The comparator's noise is presumed minimal in comparison to the total voltage out of the amplifiers, whereas the noise prior to these gets amplified and is hence significant. The minimum accepted SNR is also determined at the comparator. Based on the use of the FEMTO DHPVA-101, we have the following equation for the SNR:

$$SNR = \frac{R_\lambda P}{N_{vEV}\sqrt{f} + R_\lambda(N_{EP}\sqrt{f} + N_{external})}$$

Where P is the power received at the APDs, R_λ is the APDs responsivity at 1550 nm, N_{vEV} is the noise equivalent voltage of the voltage amplifiers, N_{EP} is the noise equivalent power of the APDs, $N_{external}$ is the external noise power and f is the sampling rate of the APDs. Since this equation relies on the input power at the APDs, we produced a link budget to analyze all sources of optical loss and gain for our transmission laser. The SNR equation provides us with a gain coefficient of $\frac{R_\lambda P}{N_{vEV}\sqrt{f}+R_\lambda(N_{EP}\sqrt{f}+N_{external})}$ for the power, which can be coupled to our link budget to determine the total SNR of the free space communications.

Based on these predictions, we can compare and validate our design choices; for example, comparing two different voltage amplifier models. We could conclude that FEMTO DHPVA-101 would produce a 3 dB higher SNR, yet both systems are predicted to produce an SNR over the required threshold.

A significant limitation of this model is the fact that it does not account for noise from polarization effects. The dual-channel nature of the OGS produces uncommon SNR requirements based on the comparator's resolution, and which will be evaluated through a separate link budget discussed later. Nevertheless, this model allows us to understand and model our capacity to receive any signal while not distinguishing between 1 and 0 bits.

FPGA System

A Digilent Zedboard with the Xilinx Zynq-7000 dual FPGA-CPU system allows the use of the chip's FPGA to perform high-speed writes from the board's input pins to the board's DDR3 memory, while the CPU periodically retrieves the updated data from memory and transmits it over Ethernet to the ground control computer.

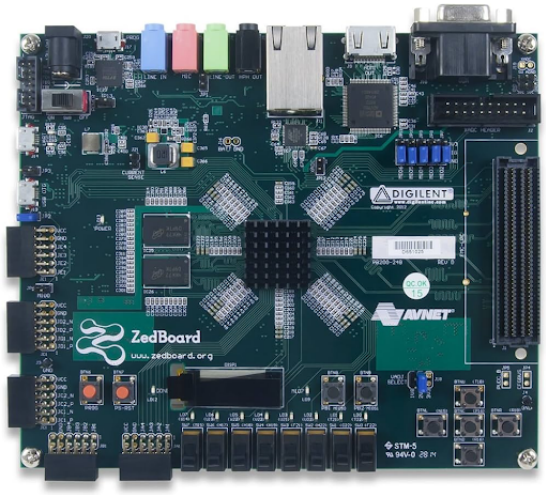

Figure 15: The Digilent Zedboard is an FPGA development board with ports allowing for connections to a variety of peripheral devices. We connect the comparator circuit with the FPGA Mezzanine Card port on the right of the board, and output data over TCP using the Ethernet port on the board.

We plan to have the FPGA store a memory address pointer which increments once per clock cycle and uses a Direct Memory Access (DMA) system connected to the data input port to write the data from the input directly to the memory location specified by the address counter. Then, a loop on the CPU will periodically read the value of the address pointer, compare it to the address from the previous iteration, and read the bytes from memory between the two addresses. Lastly, the Zedboard will act as a TCP server and send a packet containing the bytes to all connected clients.

Error Correction

The use of error correction allows for an operable communication link under a lower SNR as intermittent errors caused by noise can be detected and corrected without interfering with the communication system. Several error correction schemes have been evaluated for integration into the communication pipeline with a specific focus on both the Hamming and Reed-Solomon code.

The Hamming code is a lightweight code capable of correcting single-bit errors and detecting two-bit errors per block, with larger block sizes allowing for fewer redundancy bits. Due to its simplicity and low computational overhead, it is well-suited for low-error, low-latency environments. However, its correction capabilities are limited, and it does not perform well in the presence of burst errors—multiple error bits which appear in sequence.

In contrast, the Reed-Solomon code is a more powerful block-based error correction scheme that is particularly effective at correcting multiple-symbol errors and is widely used in storage media, space communications, and digital broadcasting. Its robustness against burst errors and adaptability to variable block sizes makes it preferable for applications with higher noise tolerance requirements. Given the expected noise characteristics of this project, where intermittent atmospheric disturbances can cause burst errors, Reed-Solomon was selected as the primary error correction scheme.

To facilitate rapid development, validation, and iteration, the error correction pipeline is first being implemented in Python. This software simulation environment enables flexible modular testing of various encoder/decoder configurations and noise models. The pipeline includes the following components:

- Source Generation: Synthetic data is generated to simulate typical Payloads.
- Encoder: The data is encoded using either Hamming, Reed-Solomon, or another chosen code, introducing redundancy necessary for correction.
- Channel Model: A simulated noisy channel introduces controlled random or burst errors to the encoded data.
- Decoder: The corrupted message is passed through the appropriate decoding algorithm in an attempt to recover the original Payload.
- Verification: The output is compared with the original data to assess the effectiveness of error correction and characterize performance under different noise levels.

This modular simulation framework allows for the controlled evaluation of error correction performance, the ability to change encoding frameworks, and the generation of diagnostic metrics.

Following successful validation of the software-based pipeline, the finalized error correction algorithm will be adapted to an FPGA. FPGAs are well-suited for hardware implementations of error-correcting codes as they can process a stream of data at rates as high as the FPGA's clock speed (e.g 33.3 MHz on the Zedboard).

Beacon Assembly

Like the OGS, the satellite also actively adjusts its body pointing and laser pointing as part of the PAT sequence. The satellite must first conduct an initial coarse body-pointing maneuver using GPS data for both the satellite and the OGS's location. However, for the satellite's fine pointing, the OGS will also provide an uplink beacon laser.

At the beginning of a transmission pass, the OGS will illuminate a high-power (10W) laser mounted on the body of the telescope. This laser will be configured with a higher beam divergence angle than the downlink lasers on the satellite. Thus, the telescope's coarse pointing along the satellite's predicted orbital path (pre-Acquisition) will be sufficient for detection by the Payload.

Based on the incidence angle of this uplink beacon to the body of the satellite, the Payload will adjust the transmission laser's FSM center the beacon laser onto the transmission laser emitter, thereby pointing the transmission laser back toward the ground station.

In designing this system, it is necessary to consider all possible noise sources which could interfere with the Payload's fine pointing system. If the SNR received by the Payload is too low, the Payload will

not be able to perform fine pointing. Thus, to increase the SNR, the beacon laser can be configured to encode a function, which the Payload's uplink beacon receiver assembly can isolate from noise.

The uplink beacon laser, for example, can be modulated by a sinusoidal wave function and the Payload can detect signals modulated at the specified frequency, effectively allowing the Payload to ignore noise from incident light. This also has the potential to be used to mitigate back reflections on the Payload.

Scintillation effects on the Payload must also be considered. While it is still unclear how scintillation can affect the SNR at the Payload's detector, we have considered possible mitigation strategies. One possible strategy includes producing a beacon beam by using four parallel sources surrounding (and parallel to) the telescope, which can significantly reduce the random jitter of the beam (Hemmati).

Ground Control

The ground control software must unify both RFGS and OGS functions, such as the telescope controls, telemetry viewer, and live data plotter, into a single, user-friendly tool ensuring ease of mission control. The control software must fulfill the following requirements:

- Operate the OGS tracking and signal decoding systems
- Establish and maintain the RFGS communication link
- Send and receive commands to and from the RFGS and OGS
- Monitor and analyze mission operations in real time
- Record and archive information from the RFGS and OGS
- Integrate external software modules like GNU Radio and GPredict
- Initiate, terminate, schedule, and automate the operations of the RFGS and OGS

PyQt GUI

Rather than use existing mission control software such as OpenMCT or OpenC3/COSMOS, we will be developing our own GUI software using Python's PyQT library. OpenMCT and OpenC3/COSMOS are both web-based tools developed in Javascript and Ruby, respectively, which makes integration with our Python-based control code challenging. For this reason, developing a proprietary GUI will save development and integration time. The OGS and RFGS will be running two independent PyQt windows which will be connected over the internet.

RFGS Control

We utilize GNU Radio to control our radio communications chain, interfacing with the TNC, transceiver, and antenna. Uplink commands are initiated by the PyQt GUI: commands are wrapped in AX.25 (carrying CSP Payloads), sent over KISS to the TNC, GFSK-modulated at 9.6 kbps, and then forwarded as audio to the transceiver for transmission. Downlink telemetry data will be received by the transceiver and then will enter the TNC where it will be demodulated and deframed into AX.25 packets. Lastly, these packets will be forwarded via KISS to the RF control computer where they will be decoded by GNU Radio and displayed on the PyQT GUI. This architecture will let us iterate quickly on packet formats and automation logic.

In our setup, GPredict runs locally on the RF control computer. GPredict will frequently pull the satellite's two-line elements (TLEs) and compute our satellite's real-time Doppler's offset and altitude-azimuth coordinates. GPredict then streams pointing commands to the antenna and pushes frequency-correction values into GNU Radio for frequency adjustments. Using GPredict will allow us to have automated beam steering and Doppler compensation without additional hardware.

In our setup, the PyQt GUI serves as the control hub, interfacing with both GNU Radio and GPredict. It establishes a ZeroMQ connection with the GNU Radio, through which downlink AX.25 PDUs are received for real-time telemetry visualization inside the GUI. Operators will also issue uplink commands inside the GUI. Simultaneously, the GUI will communicate with GPredict via its built-in TCP interface to acquire real-time orbital parameters like azimuth, altitude, and Doppler shift corrections, which are then relayed to the antenna controller and injected into GNU Radio's signal processing chain. This unified application allows operators to monitor telemetry and manage RF communications within one interface.

OGS Control

The OGS Control software will be integrated with the following modules:

- Telescope Controls: Provides a focused interface for slewing, tracking, and fine-pointing the telescope in synchronization with RF passes.
- Data Plotter: Allows for viewing of a graph of the telemetry channel's value over time. Includes live and log modes and multiple panels (up to 4) for easy comparison. This tool can also plot local archived data.
- Command Center: Allows for the sending of standard or custom commands to the OGS.
- Record and On/Off Buttons: The On/Off buttons provide direct control over both stations' power. Processes can be shut off in the case of an emergency. The record button allows for the recording of incoming data. All data is archived once the recording is stopped.

Feasibility of Space-to-Ground CPolSK Optical Communications

While on-off keying or PPM are concerned with intensity related noise to determine SNR, our two-channel system introduces a new kind of noise: polarization noise. Polarization noise is defined as the noise produced by an alteration of the expected polarization state. This is primarily produced by the creation of elliptically polarized light which will result in a signal being detected on both the 1 and 0 bit channels of the Signal Decoding Assembly.

Polarization noise can then produce an unwanted signal that needs to be filtered out through the comparator circuit. Such a signal can only be filtered out to the maximum resolution of a comparator IC, as any smaller difference between the two signals would not be comparable. This implies that there is a maximum requirement for the ellipticity acceptable at the detectors in the OGS. Hence, understanding the effects of the free space optical communications channel on circular polarization—what we call a polarization link budget—is crucial to the success of our mission.

In order to understand these effects, we must investigate the effects of the Payload, OGS and atmosphere on circular polarization. We will characterize these by measuring the transformation of known polarization states through different parts of these channels, and then characterizing these transformations in terms of Mueller matrices. This will allow us to predict the transformation on any physical Stokes vector.

Ellipticity requirements on the OGS

To predict the success of the PULSE-A communications system, the Mueller matrix transformation must abide by a given ellipticity requirement intrinsic to the OGS's design. This can be determined from an ellipticity requirement on the OGS, provided by analyzing the maximum allowable SNR on the two-channel system.

Any generalized polarization state

$$\vec{E} = \begin{pmatrix} E_x \cos(\omega t - kz) \\ E_y \cos(\omega t - kz + \phi) \end{pmatrix}.$$

can be expressed as a linear combination of left- and right-handed circularly polarized light, $\vec{E} = a\vec{E_L} + b\vec{E_R}$. We have derived that the expressions for a and b are:

$$a = \frac{E_x + E_y \frac{\cos(\omega t - kz + \phi)}{\sin(\omega t - kz)}}{2},\ b = \frac{E_x - E_y \frac{\cos(\omega t - kz + \phi)}{\sin(\omega t - kz)}}{2}.$$

The voltage out of the APD is $V \propto I_{APD} \propto |\vec{E}|^2$, where I_{APD} is the incoming intensity. We define the signal-to-noise ratio of the two-detector system as the ratio of the received intensities. We can compute the SNRs of the APDs:

$$SNR_L = \frac{I_L}{I_R} = \frac{|a|^2}{|b|^2}, \qquad SNR_R = \frac{I_R}{I_L} = \frac{|b|^2}{|a|^2}$$

We can now express the SNRs in terms of the minimum detectable voltage difference. For the left-handed APD, we define this difference as $V_{res} := V_L - V_R$. Dimensional analysis shows $[V_R] = [I_R A_{eff} R]$, where A_eff is the effective area of the ADP and R is the responsivity. It then follows that $SNR_L = \left| \frac{E_x + E_y \frac{\cos(\omega t - kz + \phi)}{\sin(\omega t - kz)}}{E_x - E_y \frac{\cos(\omega t - kz + \phi)}{\sin(\omega t - kz)}} \right|^2$ which implies that, at minimum, $|a|^2 = \frac{V_{\text{res}}}{\frac{1}{2} c\varepsilon_0 \cdot A_{\text{eff}} \cdot R} + |b|^2$. Similarly, for the right-handed APD, we obtain $SNR_R = \left| \frac{E_x - E_y \frac{\cos(\omega t - kz + \phi)}{\sin(\omega t - kz)}}{E_x + E_y \frac{\cos(\omega t - kz + \phi)}{\sin(\omega t - kz)}} \right|^2$ which implies $|b|^2 = \frac{V_{\text{res}}}{\frac{1}{2} c\varepsilon_0 \cdot A_{\text{eff}} \cdot R} + |a|^2$. This gives us a requirement on the ellipticity coefficients, a and b.

It should be noted, however, that this is an idealized model of the two-detector system, as it doesn't take into account the internal noise from each of the detectors. Hence, this model will only represent a part of the full link budget and we plan to incorporate it with other noise factors.

It is convenient to express a and b in terms of Stokes' parameters, which are observables of the electromagnetic wave and are hence easier to measure in practice.

$$\begin{bmatrix} S_0 \\ S_1 \\ S_2 \\ S_3 \end{bmatrix} = \begin{bmatrix} E_x^2 + E_y^2 \\ E_x^2 - E_y^2 \\ 2E_x E_y \cos\phi \\ 2E_x E_y \sin\phi \end{bmatrix}, \; S_0^2 \geq S_1^2 + S_2^2 + S_3^2$$

We can express the quantities E_x, E_y, ϕ in terms of Stokes' parameters, which gives a and b as

$$a = \frac{\sqrt{\frac{S_0+S_1}{2}} + \sqrt{\frac{S_0-S_1}{2}} \left[\frac{\cos(\omega t - kz + \arctan(S_3/S_2)}{\sin(\omega t - kz)}\right]}{2}$$

$$b = \frac{\sqrt{\frac{S_0+S_1}{2}} - \sqrt{\frac{S_0-S_1}{2}} \left[\frac{\cos(\omega t - kz + \arctan(S_3/S_2)}{\sin(\omega t - kz)}\right]}{2}$$

Fiber Experiment

We first attempted to characterize polarization transformations by analyzing the Payload's optical fibers. These are the major sources of polarization noise in the Payload system, as the remainder of the system is well-documented; or, alternatively, it will have to be characterized through the use of a complete prototype of the optical system.

To determine the transformation of a polarization maintaining (PM) PANDA fiber, we coupled linearly polarized light into the fiber at an angle θ to the PM axis of the fiber. The light coupled in is linearly polarized as this is what is expected in the Payload. Then, using a Thorlabs PAX1000 polarimeter we measured the polarization state. As expected, we saw trends in ellipticity with a $\frac{\pi}{2}$ period. The following graph depicts the ellipticity of a final polarization state after inputting a linear polarization state at an angle θ to the PM axis of the fiber.

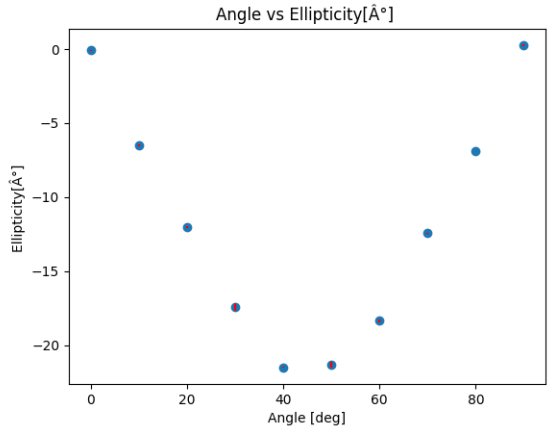

Figure 16: Ellipticity of polarized light exiting a PM fiber against the angle between the incident polarization state and the PM axis of the fiber. The trend is 2 periodic. Data points were collected for an average of data over a 30 second integration time.

In order to complete our transformation model using Mueller matrices, we will need to perform the same measurements while coupling circularly polarized light into the fibers. This is because you need at least four non-degenerate non-zero states (i.e. elliptical polarization states) to compute a Mueller matrix . Understanding this requirement to model the transformations with Mueller matrices allows us to perform other experiments more precisely. These Mueller matrices can be used to predict transformations by the optical fiber on linear polarization states which correspond to the binary data modulated at the Payload. Hence, we will be able to cross verify our results from the above transformations with our Mueller matrix model.

Telescope Experiment

We anticipate that the OGS's telescope may pose a potential problem in introducing polarization noise as coatings or small deformities in the primary mirror could cause transformations in an initial polarization state. Hence, we will be categorizing the OGS's telescope using the Mueller matrix method.

To perform this experiment, we must input a collimated beam of left- and right-handed circular polarization states, as well as other elliptical or linear polarization states into the telescope. Producing an 11-inch collimated beam is not feasible within a laboratory space. Thus, our beam would be only 2" wide.

If we expect the transformations to be symmetrical over the entire telescope primary mirror, we will not need to scan over the telescope's area. On the other hand, if we take the contributions of mirror imperfections to be significant, we will need to scan over the entire area of the telescope. This could also result in a more complex model, in which the interference of asymmetric transformations would need to be considered.

Long Distance Experiment

Likely the largest and most unpredictable part of our communications system is the atmosphere. The article "Analysis of CPolSK-based FSO system working in space-to-ground channel" suggests that there are small changes in the polarization state when using CPolSK for space-to-ground optical communications—a major benefit of this modulation scheme. We intend to replicate these results over a smaller horizontal distance, which will simulate the approximately 500km distance of our orbit due to the larger atmospheric density at sea level and produce a Mueller matrix model for this.

Further Experiments

While these three experiments outlined are used to determine some of the largest expected sources of polarization noise, we will continue to characterize our FSO communications system beyond these. This will include producing Mueller matrices for a prototype Payload and OGS, allowing us to finalize a model for the entire system. Then, coupling this system to our ellipticity requirements and single channel intensity link budget, we should be able to establish the viability of communications, and correct for any issues with increased sensitivity in detectors, manufacturing, circuitry, coatings or any other source of polarization noise.

Conclusion

As PULSE-A approaches its CDR, understanding our design's capacity to track, collect and decode the polarization modulated transmission is crucial for verification of our ground station system. This primarily includes successfully tracking the ISS with our telescope, building and characterizing a prototype of the OGS's Polarization State Preparation Assembly, and characterizing the Payload and atmosphere. These factors will validate the capacity of the OGS to perform novel space-to-ground polarization-based optical communications. Furthermore, we will be able to test our non-FSO components to their fullest extent, such as our Signal Decoding assembly and RFGS, which we intend to prototype and test for upcoming design reviews.

Acknowledgemetns

PULSE-A's launch is supported through the CubeSat Launch Initiative as part of NASA's Educational Launch of Nanosatellites (ELaNa) program, notice ID #NNH23ZCF001. The project's work is supported by the University of Chicago Pritzker School of Molecular Engineering, Department of Physics, Physical Sciences Division, Department of Astronomy and Astrophysics, as well as the Chicago Quantum Exchange. The project is further supported by the University of Chicago Women's Board and Select Equity, LLC. We also thank our numerous private donors who supported this work.

References

Hemmati, Hamid. Near-Earth Laser Communications. CRC Press, 2021.

Riesing, Kathleen Michelle. "Portable Optical Ground Stations for Satellite Communication." MIT, MIT, 2018.

Su, Yuwei, and Takuro Sato. "Analysis of CPOLSK-Based FSO System Working in Space-to-Ground Channel." ScienceDirect, 22 Nov. 2017, www.sciencedirect.com/science/article/pii/S0030401817310428#d1e830. Accessed 09 June 2025.

Tian, Hui. "Noise Analysis in CMOS Image Sensors." Stanford, 2000.